frontiers | Frontiers in Mechanical Engineering

TYPE Original Research
PUBLISHED 27 March 2023
DOI 10.3389/fmech.2023.1128447

OPEN ACCESS

EDITED BY
Dairene Uy,
Shell, United States

REVIEWED BY
Peter M. Lee,
Southwest Research Institute (SwRI), United States
Swarn Jha,
Texas A&M University, United States

*CORRESPONDENCE
Stefan Hofmann,
stefan.hs.hofmann@tum.de

SPECIALTY SECTION
This article was submitted to Engine and Automotive Engineering, a section of the journal Frontiers in Mechanical Engineering

RECEIVED 20 December 2022
ACCEPTED 02 March 2023
PUBLISHED 27 March 2023

CITATION
Hofmann S, Lohner T and Stahl K (2023), Influence of water content on elastohydrodynamic friction and film thickness of water-containing polyalkylene glycols.
Front. Mech. Eng 9:1128447.
doi: 10.3389/fmech.2023.1128447

Influence of water content on elastohydrodynamic friction and film thickness of water-containing polyalkylene glycols

Stefan Hofmann*, Thomas Lohner and Karsten Stahl

Department of Mechanical Engineering, School of Engineering and Design, Gear Research Center (FZG), Technical University of Munich, Munich, Germany

Lubricants with a functional water portion have demonstrated a drastic reduction in friction under elastohydrodynamic lubrication conditions. With water-containing polyalkylene glycols, superlubricity with coefficients of friction <0.01 have been measured in model and gear contacts. In addition to the low friction, their calorimetric properties make them particularly interesting for application in electrified vehicles because the liquid can simultaneously serve as lubricant for the gearbox and coolant for the electric motors and the power electronics. In this study, the influence of water content between 8 wt% and 40 wt% of water-soluble polyalkylene glycols on friction and film thickness in elastohydrodynamically lubricated rolling-sliding contacts such as in gears and bearings is investigated. A polyalphaolefine oil is used as a reference. Friction has been measured on a ball-on-disk tribometer and film thickness on an optical tribometer. For a water content of 40 wt%, superlubricity with coefficients of friction down to 0.004 are found. The decrease in friction is up to 95% compared to the polyalphaolefine reference. The measured film thickness decreases with increasing water content. For a water content of 8 wt%, the film thickness is similar to that of the polyalphaolefine reference while at the same time friction is still reduced by 81%. Depending on the friction and film thickness requirements of a specific tribosystem, the water content of a water-containing polyalkylene glycol can be chosen accordingly.

KEYWORDS

aqueous lubrication, superlubricity, EHL, polyalkylene glycols, film thickness

1 Introduction

Reducing friction in powertrains is of primary importance in saving energy and reducing carbon emissions (Holmberg and Erdemir, 2017; Woydt, 2021). Additionally, the sustainability of the entire value chain of novel lubricants is increasingly important because resources are limited and their extraction is energy intensive. The value chain covers the entire lifetime of a product from production and operation to disposal or reuse. In this context, lubricants based on water, polyalkylene glycol or glycerol were investigated as

Abbreviations: EHL, Elastohydrodynamic lubrication; PAO, Polyalphaolefine; PAG, Polyalkylene glycol; PAGW, Water-containing polyalkylene glycol; BUT, Brno University of Technology; ISO, International Standard Organization; VG, Viscosity grade; BEV, Battery electric vehicle.

environmentally friendly alternative to conventional lubricants (Voorst and Alam, 2000; Escobar, 2008; Shi et al., 2014). Such lubricants are often referred to green lubricants (Shi et al., 2014).

In battery electric vehicles (BEV) in particular, holistic powertrain designs with high efficiency are accompanied by low energy consumption and hence higher ranges or lower weights depending on the system design goals. Morhard et al. (2021) investigated the use of a single water-containing liquid for gearbox lubrication and cooling of motors and power electronics in a high rotational speed electric powertrain. The favorable calorimetric properties such as high specific heat capacity and thermal conductivity (Schmidt et al., 2006; Sagraloff et al., 2019; Luther, 2021) make water-containing liquids suitable for a holistic thermal management in electrified powertrains. Nevertheless, there remain a number of outstanding challenges before such lubricants can be used in practice (Morhard et al., 2022). For example, water evaporation as well as corrosion and material incompatibilities have to be avoided.

The load-dependent power losses of gears or bearings are related to the friction in their elastohydrodynamically lubricated (EHL) rolling-sliding contacts. Especially in BEVs, the trend is towards higher rotational speed of the electric motors (Schweigert et al., 2020; Morhard et al., 2021), making load-dependent power losses arising from the gearbox become highly relevant. In addition to BEVs, the reduction of load-dependent power losses is also very important in industrial applications. The substitution of mineral oils with synthetic oils such as polyalphaolefines (PAO) or polyalkylene glycols (PAG) can already significantly reduce EHL friction (Mayer, 2013; Ziegltrum et al., 2017). The use of lubricants with very low kinematic viscosity makes possible a further reduction in friction, but at the expense of limited film thickness. This can shift lubrication regimes to mixed and boundary lubrication provoking surface wear.

Lubricants with a functional water portion can achieve superlubricity in rolling-sliding EHL contacts while at the same time being capable of lubricant film formation (Zhang et al., 2012; Shi et al., 2014; Yilmaz et al., 2019a). Water-containing lubricants can be categorized as a subcategory of aqueous lubricants (Spencer, 2014; Ge et al., 2019; Han et al., 2022) with water portions of up to 90 wt% (Wang et al., 2016; Sagraloff et al., 2019). In addition to water-soluble PAGs (Zhang et al., 2012; Wang et al., 2016; Ge et al., 2018; Yilmaz et al., 2019a; Yilmaz et al., 2019b; Liu et al., 2019; Burbank et al., 2020), glycerol (Cheng et al., 2013; Li et al., 2013; Shi et al., 2014; Tamayo et al., 2022) is often used as a water-soluble liquid. For both base stocks, friction measurements in tribometers show coefficients of friction in the superlubricity regime with values <0.01 (Hirano and Shinjo, 1990). For water-containing PAGs, Yilmaz et al. (2019a) observed only slightly lower film thickness than for PAOs, which was attributed to the higher density. No information on the water content was provided. Yilmaz et al. (2019b) also measured superlubricity in gears. Sedlmaier et al. (2020) conducted experiments on a BEV test rig with the lubricants investigated by Yilmaz et al. (2019a, b) and found a reduction of power losses of up to 74% compared to PAOs.

Habchi et al. (2011) carried out numerical investigations on the influence of the water content of glycerol on friction and film thickness in EHL contacts. The results show reducing coefficients of fluid friction with increasing water content up to 40 wt%, at which superlubricity was found for all considered operating conditions. However, the film thickness is shown to be approximately one order of magnitude lower for 40 wt% water when compared to pure glycerol. A similar trend was observed in the experimental investigations of Shi et al. (2014) on a ball-on-disk tribometer with water-containing glycerol of up to 20 wt% water. For higher water contents of up to 50 wt%, limited film thickness lead to a transition from fluid film to mixed and boundary lubrication with strongly increasing coefficients of friction. Pressure-viscosity coefficients derived from film thickness measurements were found to decrease with increasing water content. Wang et al. (2016) investigated the influence of water content of water-soluble PAGs on a ball-on-disk tribometer subject to reciprocating motion. Coefficients of friction as low as 0.0023 were reported for 50 wt% water. In the experimental studies of Liu et al. (2019), water-containing PAGs with different molecular weights of PAG and water concentrations were investigated on a ball-on-disk tribometer, as previously used by Wang et al. (2016). Liu et al. (2019) showed that the time to achieve stable superlubricity depends on the concentrations of PAG and water and that with increasing molecular weight, the threshold water concentration for reaching superlubricity increases. Burbank et al. (2020) conducted friction and film thickness measurements for water-containing PAGs on a ball-on-disk tribometer under rolling-sliding conditions. Superlubricity was found over a wide range of operating conditions. Almost no influence of the load on friction was observed in fluid film lubrication regime. Tamayo et al. (2022) conducted friction measurements with water-containing glycerol with 5 wt% water and a combination of 5 wt% water and additionally 30 wt% glycol with glycerol as base stock. The lubricants were prepared so that they reached a comparable film thickness in boundary lubrication regime. Both lubricants reduced friction and mild wear compared to PAO.

The detailed mechanisms resulting in superlubricity with water-containing lubricants in EHL contacts are subject of research. A group of authors (Li et al., 2013; Wang et al., 2016; Liu et al., 2019) explained the superlubricity in fluid film lubrication regime as being due to surface interactions with water-containing PAGs resulting in the formation of unbonded layers of water with low shear resistance within the fluid film. Ge et al. (2018) proposed the formation of a stable tribofilm by water-containing PAGs, which allows a parallel orientation of fluid molecules within the fluid film. Also, after replacement of the water-containing PAG with a PAO, Ge et al. (2018) demonstrated superlubricity. It has also been shown that water-containing lubricants feature significantly lower pressure-viscosity coefficients when compared to conventional lubricants (Schmidt et al., 2006; Zhang et al., 2012; Shi et al., 2014; Tamayo et al., 2022). Water exhibits nearly no dependency of kinematic viscosity on pressure (Gohar, 2001). Hence, the effective viscosity in the contact zone of EHL contacts might be significantly lower when compared to conventional oils. This can also be causal for low shear resistance and superlubricity (Habchi et al., 2011).

The literature review reveals a high level of research activity in the field of superlubricity in EHL contacts with water-containing lubricants. However, there is a lack of systematic investigations on the influence of the water content on friction and film thickness. Most studies (Habchi et al., 2011; Li et al., 2013; Shi et al., 2014) have investigated the influence of the water content for a given PAG or glycerol. Hence, the viscosity differs by up to two orders of magnitude

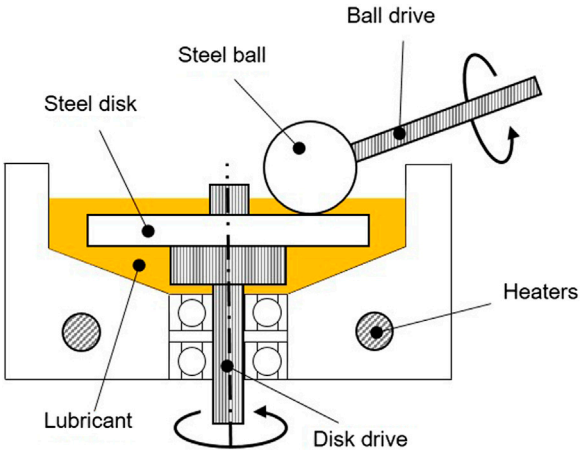

FIGURE 1
Schematic representation of the mechanical layout of the MTM2 test chamber.

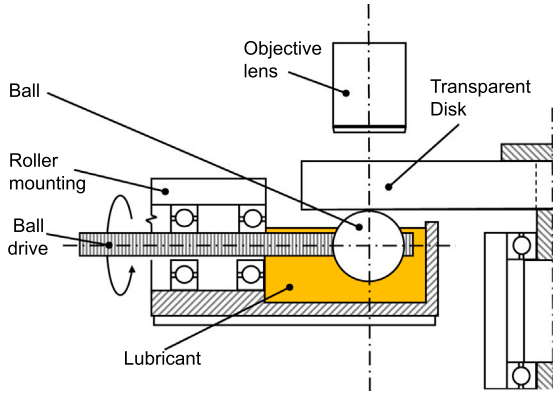

FIGURE 2
Schematic representation of the mechanical layout of the optical EHL tribometer test chamber based on (Omasta et al., 2018; Yilmaz et al., 2019a).

in comparison of the considered water-containing lubricants (Shi et al., 2014). This study experimentally investigates the influence of the water content of PAGs on friction and film formation in EHL rolling-sliding contacts such as in gears and bearings. The kinematic viscosity of the considered water-containing PAGs (PAGW) is kept constant. The correlation of friction and film thickness is addressed. The results presented are an extended version of an abstract published at the 63rd German Tribology Conference (GfT), 26.–28. September 2022, Göttingen, Germany.

2 Materials and methods

For friction measurements, a MTM2 ball-on-disk tribometer is used. Film thickness is determined using an optical EHL ball-on-disk tribometer. Polished surfaces are used so that the study is focused on fluid friction. The tribometers as well as the operating conditions, lubricants and experimental procedure are described.

2.1 Ball-on-disk tribometer for friction measurement

Friction measurements are performed on the ball-on-disk tribometer MTM2 from PCS Instruments Ltd., London, United Kingdom. Figure 1 shows a schematic representation of the test chamber. The ball is loaded via a leaf spring so that it is pressed against the face of the disk. The ball and disk are driven independently, so that various rolling-sliding conditions can be adjusted. The frictional force in the EHL contact between the two specimens is measured by a load cell located at the driving shaft of the ball. In this study, a 3/4 inch diameter ball is paired with a disk. Both test specimens are made of 100Cr6 (AISI 52100) with polished surfaces. Tactile roughness measurements are performed transversally to the running track of the ball and disk and give a root mean square surface roughness of the ball of Rq_1 = 10.5 nm and a corresponding disk roughness of Rq_2 = 9.0 nm. As shown in Section 4.3, this results in fluid film lubrication regime with fully separated surfaces for almost all of the operating conditions under consideration. The tests are conducted in a fully-flooded lubricant chamber. The lubricant temperature ϑ_{Oil} is controlled by heaters embedded in the pot of the test chamber and is measured in the lubricant sump next to the disk.

For each friction curve, the slide-to-roll ratio *SRR* is varied from 0.0 (pure rolling) to 1.0 at constant mean speed v_m. The *SRR* is defined as the ratio of sliding speed v_g to mean speed v_m

$$SRR = \frac{|v_g|}{v_m},$$

where the sliding speed v_g is the difference between the speed of the ball 1 and the speed of the disk 2. The mean speed v_m is the mean of the surface speed of ball 1 and disk 2:

$$v_g = v_1 - v_2$$
$$v_m = \frac{v_1 + v_2}{2}.$$

For the friction measurements, the "unidirectional traction step" of MTM2 software is used. Hence, the measured coefficients of friction correspond to the mean value for negative and positive *SRR*.

2.2 Optical EHL tribometer for film thickness measurement

EHL film thickness measurements are performed on an optical EHL tribometer using thin film colorimetric interferometry (Hartl et al., 1997). It is also a ball-on-disk tribometer. The EHL tribometer has been manufactured by Brno University of Technology (BUT) and has already been used in earlier studies with water-containing lubricants (Yilmaz et al., 2019a). Figure 2 shows the schematic representation of the EHL tribometer. The following description is based mainly on the works of Omasta et al. (2018) and Yilmaz et al. (2019a).

TABLE 1 Properties of the investigated lubricants (*Kinematic viscosity at 100 °C extrapolated for water-containing lubricants).

	$PAGW_{8wt\%}$	$PAGW_{20wt\%}$	$PAGW_{40wt\%}$	PAO-05
Kinematic viscosity $\nu(40°C)$ in mm^2/s	23.34	23.18	20.38	20.40
Kinematic viscosity $\nu(100°C)$ in mm^2/s	4.0	4.3	4.4	5.0
Density ρ in kg/m^3	1130	1120	1100	840
Water content in wt%	8	20	40	0
Refractive index n at 20°C	1.4524	1.4400	1.4148	1.4585
Base oil	PAG	PAG	PAG	PAO

TABLE 2 Operating conditions at MTM2 and EHL tribometer.

	MTM2 tribometer	EHL tribometer
Hertzian contact pressure p_H in N/mm^2	800; 1000; 1200	1200
Mean speed v_m in m/s	1.0. . .2.5	0.5. . .2.0
Slide-to-roll ratio *SRR*	0.0. . .1.0	0.0

In the EHL tribometer a disk is loaded via a dead weight lever mechanism against a one inch diameter ball. The ball and disk are each individually driven by a speed-controlled electric motor to allow continuous variation of the speeds. In this study, the disk is made of sapphire and the ball of 100Cr6 (AISI 52100). The surfaces of both specimens are polished to achieve a surface roughness Ra <0.01 µm. The mean speed v_m, sliding speed v_g and *SRR* are defined identically as for the MTM2 tribometer (see Section 2.1). The ball rotates in a temperature-controlled lubricant reservoir, which supplies the contact between disk and ball. The lubricant temperature ϑ_{oil} is measured by a thermocouple directly located in the inlet zone of the EHL contact.

For evaluation of EHL film thickness, the interference pattern within the contact is tracked by an industrial microscope and evaluated using thin film colorimetric interferometry. Details on the measurement principle can be found in references (Hartl et al., 1997; Omasta et al., 2018).

2.3 Lubricants

Three water-containing lubricants with different water content are considered. A polyalphaolefine oil is considered as a reference. All lubricants are of grade ISO VG 22. The water-containing lubricants are based on water-soluble PAGs. The constant viscosity grade is achieved by different PAG chain lengths. Furthermore, additives such as extreme-pressure, anti-wear, foam inhibitor, anti-freeze and corrosion protection are added. The water contents under consideration were determined by Karl-Fischer titration and are 8 wt% for $PAGW_{8wt\%}$, 20 wt% for $PAGW_{20wt\%}$ and 40 wt% for $PAGW_{40wt\%}$. The water content of 8 wt % represents an azeotropic state resulting from the hygroscopic properties of water-soluble PAGs. The maximum water content of 40 wt% was chosen because literature shows very poor lubricant film formation capability for higher water content. The reference PAO-05 was also considered by Yilmaz et al. (2019a). The properties of all investigated lubricants are listed in Table 1.

2.4 Operating conditions

The speed and contact pressure are varied while maintaining a constant oil temperature of ϑ_{Oil} = 40 °C and are listed in Table 2. On the MTM2, mean speed v_m and slide-to-roll ratio *SRR* are varied for three Hertzian contact pressures p_H, while on the EHL tribometer only the mean speed v_m is varied under constant load and pure rolling conditions.

2.5 Experimental procedure

On the MTM2 tribometer, for each mean speed under consideration, the system is heated up to ϑ_{Oil} = 40°C under no-load and *SRR* = 0.0 conditions to ensure a quasi-stationary temperature distribution. Then the load is applied and friction curves are recorded as a function of *SRR*. The first test sequence is conducted at a contact pressure of p_H = 1200 N/mm^2. In doing so, the mean speed is stepwise decreased from v_m = 2.5. . .1.0 m/s. The second and third test sequence are conducted at contact pressures of p_H = 1000 N/mm^2 and 800 N/mm^2. The coefficients of friction shown in Section 3 and Section 4 represent the mean value obtained for positive and negative *SRR* (see Section 2.1). For material pairings with similar thermal effusivity, the kinematic conditions in terms of negative or positive *SRR* have a negligible effect on the coefficient of friction (Liu et al., 2020).

On the optical EHL tribometer, for each mean speed under consideration, the system is heated up to ϑ_{Oil} = 40°C under no-load conditions to ensure a quasi-stationary temperature distribution. Then the load is applied and the lubricant film thickness measured while increasing the mean speed incrementally from v_m = 0.5 to 2.0 m/s. Each lubricant film thickness presented in Section 3 and Section 4 represents the mean arithmetic value of three single measurements. Evaluation of measurement repeatability gives a maximum deviation of 3.3 nm for PAO-05, 12.6 nm for $PAGW_{8wt\%}$, 6.4 nm for $PAGW_{20wt\%}$ and 7.7 nm for $PAGW_{40wt\%}$, respectively.

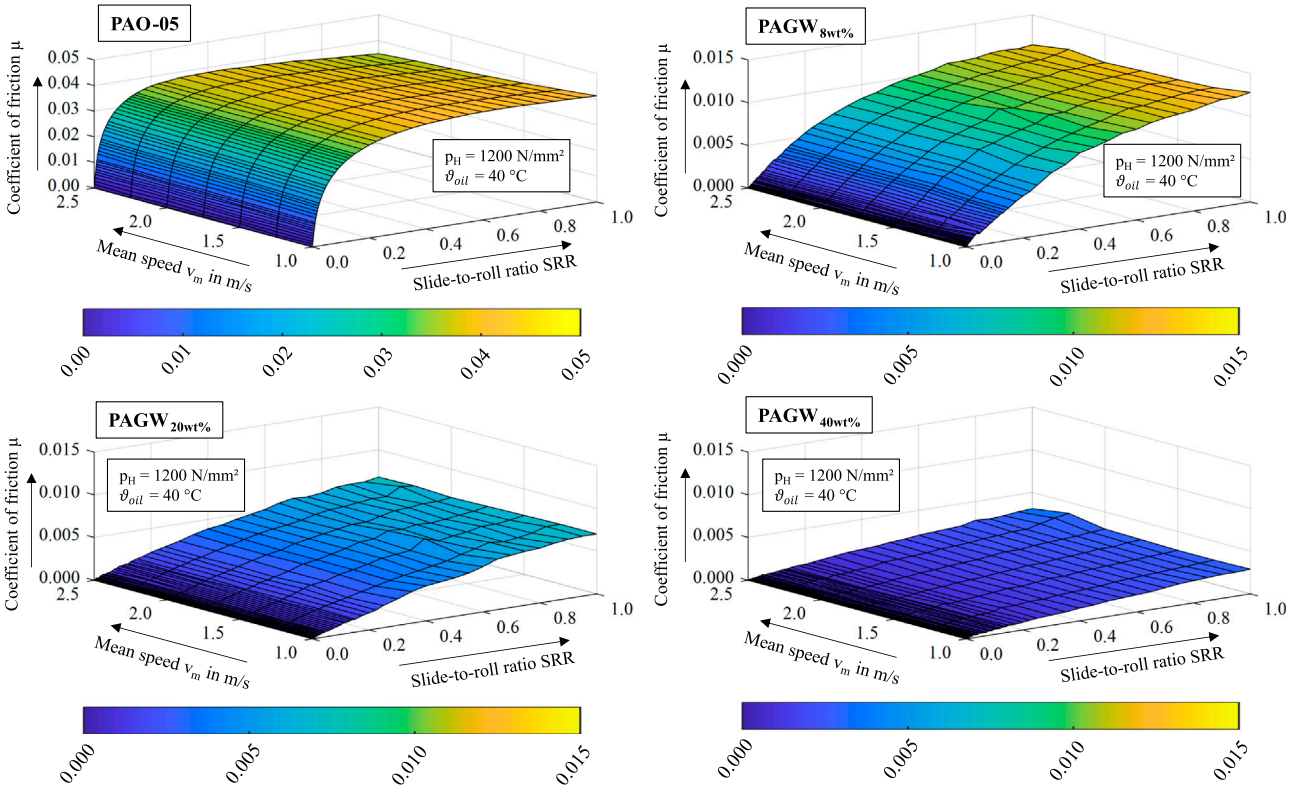

FIGURE 3
Friction maps in comparison of the investigated lubricants at p_H = 1200 N/mm² and ϑ_{Oil} = 40°C.

For water-containing lubricants, the evaporation of water needs to be prevented or controlled within specified limits to avoid a change in properties. The tribometer design and test procedure have a significant influence. For the water-containing lubricants $PAGW_{8wt\%}$, $PAGW_{20wt\%}$ and $PAGW_{40wt\%}$, the high ratio of lubricant volume to free surface in combination with relatively long heating and conditioning periods in the optical EHL tribometer can cause water evaporation. The actual measurement of the film thickness only takes about 5 minutes per lubricant. Therefore, the EHL tribometer is first calibrated and heated up with a flushing PAGW until the desired steady-state oil temperature has been achieved. Then a separate metallic vessel is heated up on a hotplate to the desired oil temperature and the water-containing lubricant is filled in. Due to the high thermal mass of the vessel, the small volume of lubricant (about 50 ml) is heated up immediately. In the next step, the flushing PAGW in the EHL tribometer is removed and replaced by the fresh tempered PAGW. The test procedure is then started immediately to prevent evaporation. In contrast to the EHL tribometer, the MTM2 tribometer has a more closed design with much shorter heating periods and testing times. Therefore, no flushing lubricants were used. Note that, in addition to evaporation, water absorption can also occur depending on the temperature and relative humidity (Zhang et al., 2012; Chen et al., 2013). For PAO-05, both the MTM2 and EHL tribometer are calibrated and heated up to the desired oil temperature without additional measures.

3 Results

The friction measurement results are presented in Section 3.1 and the film thickness measurement results are presented in Section 3.2.

3.1 Friction

Friction characteristic results for the considered lubricants are presented in Section 3.1.1. The influence of contact pressure is presented in Section 3.1.2, and that of mean speed in Section 3.1.3.

3.1.1 Characteristics

Three-dimensional friction maps with the coefficient of friction μ plotted against the mean speed v_m and slide-to-roll ratio SRR illustrate the results of the friction measurements. Figure 3 shows the friction maps for the reference oil PAO-05 and the three considered PAGWs at p_H = 1200 N/mm² and ϑ_{Oil} = 40°C.

For PAO-05, the friction curves per mean speed present a typical trend known for EHL fluid friction with typical oils, e.g., (Bader et al., 2017; Burbank et al., 2020). For very low values of SRR, a linear (Newtonian) regime is observed. With increasing SRR, a non-linear (shear-thinning) regime occurs, in which the coefficient of friction increases digressively until a maximum of the coefficient of friction at $\mu_{max} \approx 0.040$ is reached for the higher mean speeds of $v_m > 1.5$ m/s. This

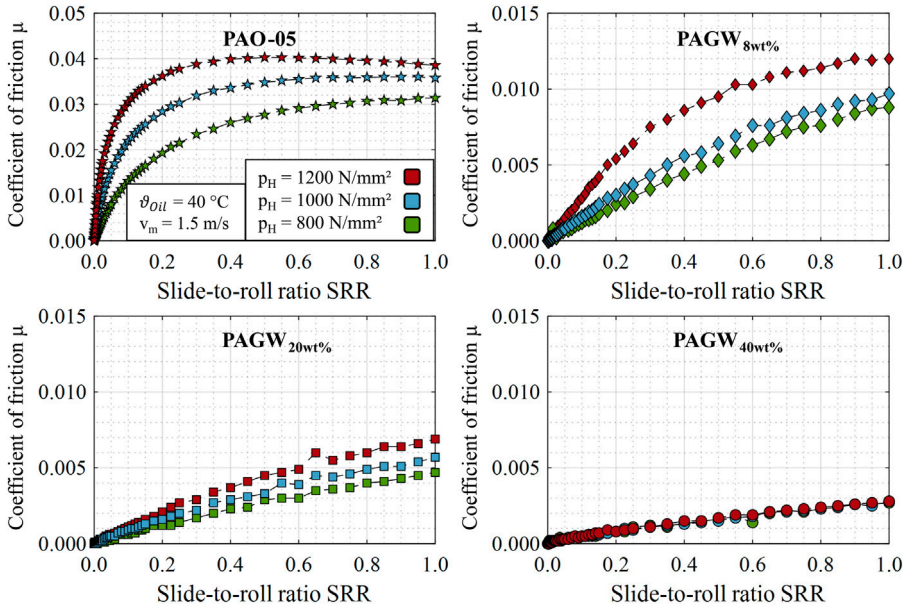

FIGURE 4
Friction curves for varying contact pressures of p_H = {800; 1000; 1200} N/mm^2 at v_m = 1.5 m/s and ϑ_{Oil} = 40°C in comparison of the investigated lubricants.

plateau is generally referred to as the limiting shear stress. For even higher *SRR*, the coefficient of friction is governed by the thermal regime and is reduced due to increasing frictional heat and local contact temperature and hence effective viscosity within the contact. Note that the thermal regime is only achieved for higher mean speeds. For lower mean speeds, the coefficient of friction generally increases the higher the *SRR*. In this context, for the investigated Hertzian contact pressure of p_H = 1200 N/mm^2, the coefficient of friction reaches a maximum of $\mu \approx 0.042$ at v_m = 1.0 m/s and *SRR* = 1.0.

For PAGW$_{8wt\%}$, the coefficient of friction first increases linearly with *SRR*, followed by a non-linear increase at higher *SRR*. For PAGW$_{20wt\%}$ and PAGW$_{40wt\%}$, the coefficient of friction increases linearly with *SRR*, which was also found by Burbank et al. (2020) and Habchi et al. (2011).

The maximum coefficient of friction μ_{max} decreases from ≈ 0.013 for PAGW$_{8wt\%}$ to ≈ 0.007 for PAGW$_{20wt\%}$ to ≈ 0.004 for PAGW$_{40wt\%}$ and is always observed at the highest investigated *SRR* value of 1.0. Hence, a higher water content results in a significant reduction in friction at constant kinematic viscosity at the oil temperature under consideration. Except for PAGW$_{8wt\%}$ at p_H = 1200 N/mm^2 and *SRR* > 0.5, superlubricity is achieved for all investigated operating conditions. The friction maps for all investigated mean speeds and loads can be found in the Supplementary Material.

3.1.2 Influence of contact pressure

The influence of contact pressure is discussed for a mean speed of v_m = 1.5 m/s. The friction maps for all investigated mean speeds and loads can be found in the Supplementary Material. Figure 4 shows the coefficient of friction plotted against SRR for the investigated lubricants for p_H = {800; 1000; 1200} N/mm^2 at v_m = 1.5 m/s and ϑ_{Oil} = 40°C.

For PAO-05, the coefficient of friction decreases with decreasing contact pressure and the profile of the friction curves changes. For p_H = {800; 1000} N/mm^2, a degressively increase with no noticeable thermal regime is observed at the mean speed under consideration. For p_H = 1200 N/mm^2, thermal effects are dominant at high *SRR* values. For PAGW$_{8wt\%}$ and PAGW$_{20wt\%}$, the coefficient of friction decreases with decreasing contact pressure, while for PAGW$_{40wt\%}$ there is no observable influence of the contact pressure on friction. A reversed test sequence compared to Section 2.5, starting at p_H = 800 N/mm^2, confirmed negligible pressure influence for PAGW$_{40wt\%}$. The investigations by Burbank et al. (2020) with water-containing PAGs also show almost no influence of load on the measured coefficient of friction. It can be seen that for PAGW$_{8wt\%}$ the profile of the friction curves changes with contact pressure. While for p_H = 1200 N/mm^2 a degressively increase over *SRR* is observed, a nearly linear increase for p_H = {800; 1000} N/mm^2 is observed both for PAGW$_{20wt\%}$ and PAGW$_{40wt\%}$. Except for PAGW$_{8wt\%}$ at p_H = 1200 N/mm^2 and *SRR* > 0.5, superlubricity is achieved for all of the investigated operating conditions.

3.1.3 Influence of mean speed

The influence of mean speed is presented for a contact pressure of p_H = 1200 N/mm^2. Figure 5 shows the coefficient of friction plotted against *SRR* for the investigated lubricants for v_m = 1.0. . .2.5 m/s at p_H = 1200 N/mm^2 and ϑ_{Oil} = 40°C.

For PAO-05, the coefficient of friction reduces with increasing mean speed in the thermal regime at high *SRR*. For PAGW$_{8wt\%}$, the coefficient of friction reduces only slightly with increasing mean speed, with the maximum difference being in the range of $\Delta\mu \approx 0.001$. For PAGW$_{20wt\%}$ and PAGW$_{40wt\%}$, the influence of the mean speed is negligible.

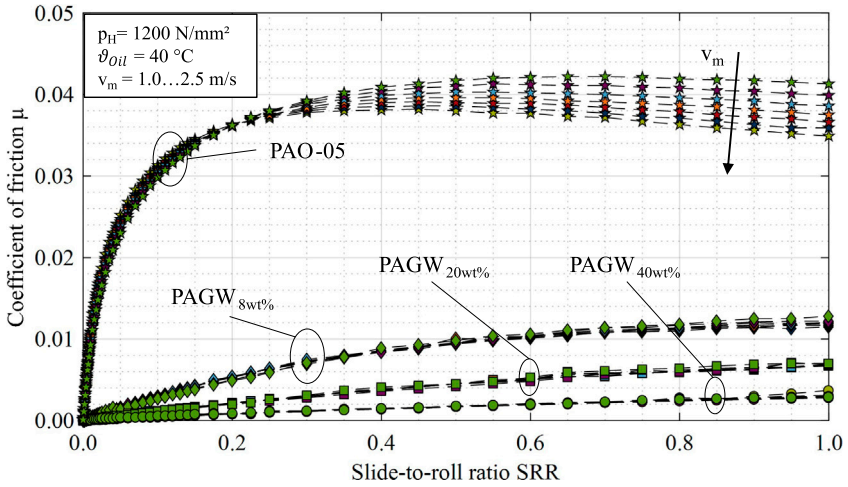

FIGURE 5
Friction curves for varying mean speeds of v_m = 1.0…2.5 m/s at p_H = 1200 N/mm² and ϑ_{Oil} = 40°C in comparison of the investigated lubricants.

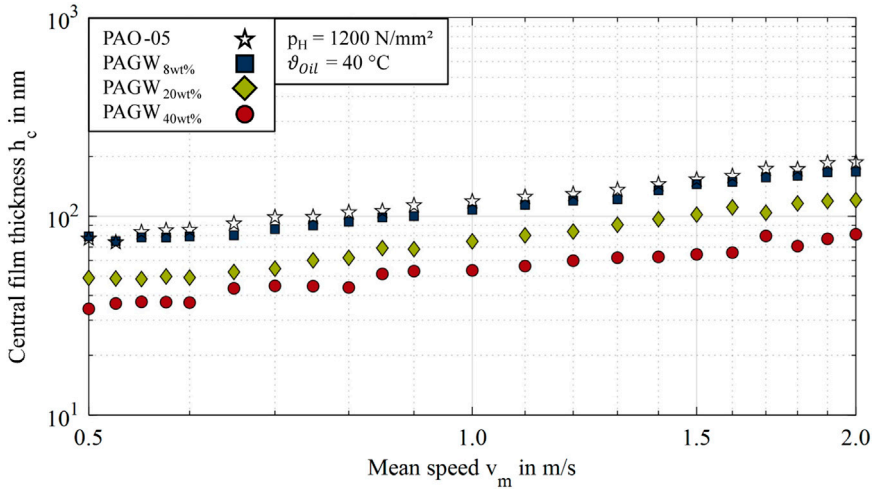

FIGURE 6
Central film thickness h_c plotted as a function of mean speed v_m at p_H = 1200 N/mm² and ϑ_{Oil} = 40°C in comparison of the investigated lubricants.

3.2 Film thickness

Figure 6 shows the measured central film thickness h_c plotted against the mean speed v_m for the investigated lubricants at p_H = 1200 N/mm² and ϑ_{Oil} = 40°C for pure rolling conditions (SRR = 0.0). The measured film thickness is plotted in double-logarithmic scale.

For all investigated lubricants, the central film thickness increases nearly linear when plotted against the mean speed in double-logarithmic scale. All lubricants are capable of forming a lubricant film. This was also observed by Yilmaz et al. (2019a) for water-containing PAGs and for water-containing glycerol by Shi et al. (2014). The film thickness decreases the higher the water content. Thus, $PAGW_{8wt\%}$ shows the maximum and $PAGW_{40wt\%}$ the minimum central film thickness. The reference oil PAO-05 exhibits only a slightly higher central film thickness than the water-containing lubricant $PAGW_{8wt\%}$. Figure 7 shows typical measured interferograms for p_H = 1200 N/mm², v_m = 2.0 m/s and ϑ_{Oil} = 40°C.

All interferograms exhibit the typical film thickness distribution known for EHL point contacts. The central film thickness h_c is located in the middle of the contact, which is surrounded by a horse-shoe shape constriction of minimum film thickness. Note that each interferogram has its own color bar as the interference pattern depends on the refractive index of the lubricants. Thereby, the refractive index reduces the higher the water content (see Table 1) as also shown by Shi et al. (2014) for water-containing glycerol.

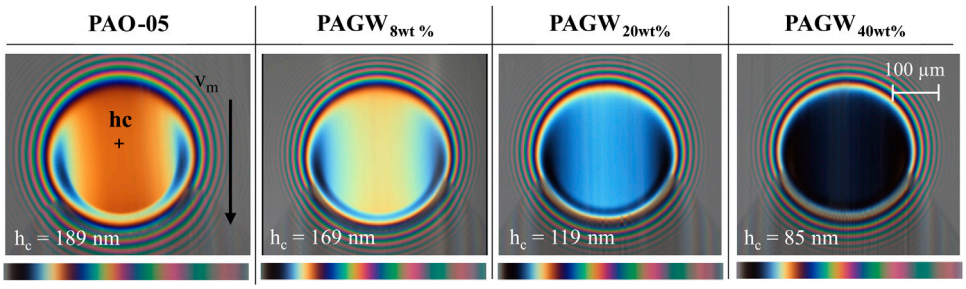

FIGURE 7
Interferograms for p_H = 1200 N/mm², v_m = 2.0 m/s and ϑ_{Oil} = 40°C in comparison of the investigated lubricants.

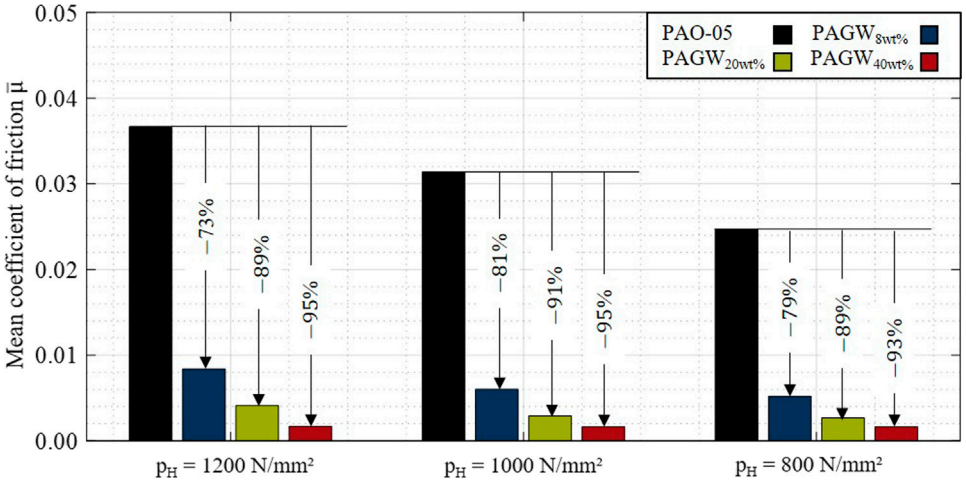

FIGURE 8
Evaluated mean coefficient of friction $\bar{\mu}$ for each contact pressure in comparison of the investigated lubricants.

4 Discussion

In the following section, the results from Section 3 are discussed in terms of the potential for friction reduction and film formation capability of the investigated water-containing PAGs.

4.1 Friction reduction and lubrication mechanism

The experimental results of Section 3.1 clearly show the potential of EHL friction reduction with PAGWs. For evaluation, a mean coefficient of friction $\bar{\mu}$ was calculated for each measured friction map. First, the mean coefficient of friction is evaluated for each friction curve at constant mean speed v_m:

$$\bar{\mu}(v_m) = \int_{SRR=0.0}^{SRR=1.0} \mu(SRR, v_m) dSRR.$$

Second, the mean values $\bar{\mu}(v_m)$ are averaged for all seven considered mean speeds:

$$\bar{\mu} = \frac{1}{7}\left(\bar{\mu}\left(1\frac{m}{s}\right) + \ldots + \bar{\mu}\left(2.5\frac{m}{s}\right)\right).$$

Figure 8 shows the calculated mean coefficients of friction $\bar{\mu}$ for each contact pressure in comparison of the lubricants under consideration.

For all PAGWs, a drastic reduction in the evaluated mean coefficient of friction $\bar{\mu}$ in comparison to PAO-05 is observed. For $PAGW_{8wt\%}$ with the lowest water content, a mean friction reduction of between 73% and 81% is observed. For $PAGW_{20wt\%}$ and $PAGW_{40wt\%}$ with higher water content an even more pronounced reduction of maximum 91% and 95% is found, whereby there is no linear trend in friction reduction with increasing water content. The contact pressure exhibits only a subordinate influence on friction reduction with PAGWs.

The experimental results in Section 3.1 also show that the characteristics of friction curves with PAGWs differ strongly

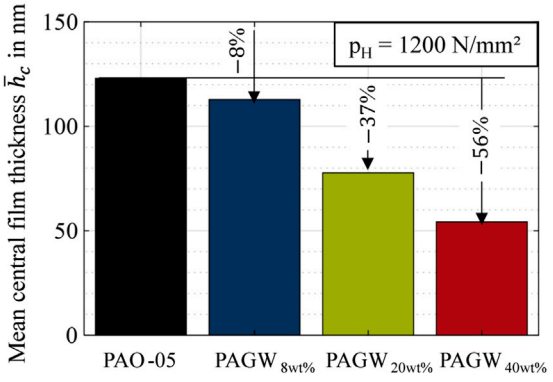

FIGURE 9
Mean central film thickness $\overline{h_c}$ in comparison of the investigated lubricants.

from the ones with PAO-05. The coefficient of friction increases slightly degressively for $PAGW_{8wt\%}$ and almost linearly as a function of *SRR* for $PAGW_{20wt\%}$ and $PAGW_{40wt\%}$, as reported in literature (Yilmaz et al., 2019a; Burbank et al., 2020). Yilmaz et al. (2019a) found steadily increasing coefficients of friction with slip ratio on a twin-disk tribometer. Flattening of the friction curves at higher speeds was attributed to the thermal effects of bulk heating.

The literature review in Section 1 shows that the low friction of water-containing lubricants is mainly attributed to layers that shear easily in the lubricant film or to low effective contact viscosity due to small pressure-viscosity coefficients. The low frictional heating within the contact for the considered PAGWs can explain the almost negligible thermal regime under the considered operating conditions. The effective contact viscosity of the PAGWs is related to the derived pressure-viscosity coefficients (see Section 4.2), which are significantly lower than those of PAO-05. The lower effective viscosity results in lower shear stress and hence lower friction. Consequently, the influence of speed and contact pressure becomes less dominant the higher the water content. The study clearly shows the strong influence of the water content on friction for similar kinematic viscosity. The underlying mechanisms resulting in superlubricity cannot be finally declared.

4.2 Film formation capability

The experimental results of Section 3.2 clearly demonstrate the ability of water-containing PAGs for lubricant film formation. For evaluation, Figure 9 shows the mean central film thickness $\overline{h_c}$ evaluated for each lubricant averaged over all considered mean speeds. While $\overline{h_c}$ for $PAGW_{8wt\%}$ is only 8% lower than for PAO-05, $\overline{h_c}$ is reduced by 37% for $PAGW_{20\%}$ and 56% for $PAGW_{40wt\%}$.

The measured EHL film thickness under pure rolling conditions discussed in Section 3.2 allows a backwards calculation of the pressure-viscosity coefficient $\alpha_p\,(40°C)$ for the investigated lubricants. In doing so, the Hamrock and Dowson equation (Hamrock and Dowson, 1976) for central film thickness in EHL point contacts is used:

$$h_c = 2.69 \cdot G^{0.53} \cdot U^{0.67} \cdot W^{-0.067}\left(1 - 0.61e^{-0.73k}\right)$$

with

$k = 1.03\left(\frac{R_y}{R_x}\right)^{0.64}$ and $\left(\frac{R_y}{R_x}\right) = 1$ for circular point contacts.

The dimensionless parameters for material (G), speed (U) and load (W) are given by

$$G = \alpha_p \cdot E',$$

$$U = \frac{\eta(\vartheta_{Oil}) \cdot v_m}{E' \cdot R_x} \text{ and}$$

$$W = \frac{F_N}{E' \cdot {R_x}^2}.$$

As all parameters for G, U and W except α_p are known, the film thickness equation can be solved for α_p. The calculation is based on the exponential curve fits of all measurement points per lubricant in Figure 6, see also (Shi et al., 2014; Yilmaz et al., 2019a). Table 3 shows the derived pressure-viscosity coefficients $\alpha_p\,(40°C)$ for the investigated lubricants.

For the water-containing PAGs, $\alpha_p\,(40°C)$ decreases from 5.9 1/GPa for $PAGW_{8wt\%}$ to 4.1 1/GPa for $PAGW_{20wt\%}$ to 3.0 1/GPa for $PAGW_{40wt\%}$. Besides water content, also the different PAG chain lengths of the water-containing PAGs influence the pressure-viscosity coefficient. The lower the pressure-viscosity coefficient, the lower is the EHL film thickness, which shifts the transition from fluid film to mixed lubrication to lower speeds, depending on the surface roughness. The reference oil PAO-05 shows $\alpha_p\,(40°C)$ = 12.2 1/GPa. The calculated pressure-viscosity coefficients of all considered PAGWs are generally in the range reported in literature (Schmidt et al., 2006; Shi et al., 2014; Yilmaz et al., 2019a).

The pressure-viscosity coefficient of PAO-05 is approximately twice that of $PAGW_{8wt\%}$. However, the central film thickness is only slightly higher (see Figure 10). This can be attributed to the higher density (approx. + 35 %) of PAGWs compared to PAO-05, which supports film formation, because the speed parameter U depends on the dynamic viscosity. Considering the reduction in the mean coefficient of friction of $PAGW_{8wt\%}$ by 81% compared to PAO-05 (see Figure 8), this is an interesting aspect in respect of EHL contact design.

4.3 Lubrication regime

The derived pressure-viscosity coefficients $\alpha_p\,(40°C)$ allow the calculation of EHL minimum and central film thicknesses for the friction measurements performed on the MTM tribometer. Considering the optical EHL tribometer, mixed lubrication can be directly excluded by the measured interferograms. The lubrication regime can be estimated by the relative film thickness λ_{rel}

$$\lambda_{rel} = \frac{h_m}{\sqrt{\left(Rq_1^2 + Rq_2^2\right)}}$$

with h_m calculated according to Hamrock and Dowson (1976). For $\lambda_{rel} > 3$, fluid film lubrication can be assumed. As the film thickness is lowest for the lowest mean speed, the investigated value of

TABLE 3 Derived pressure-viscosity coefficients.

	$PAGW_{8wt\%}$	$PAGW_{20wt\%}$	$PAGW_{40wt\%}$	PAO-05
α_p (40°C) in 1/GPa	5.9	4.1	3.0	12.2

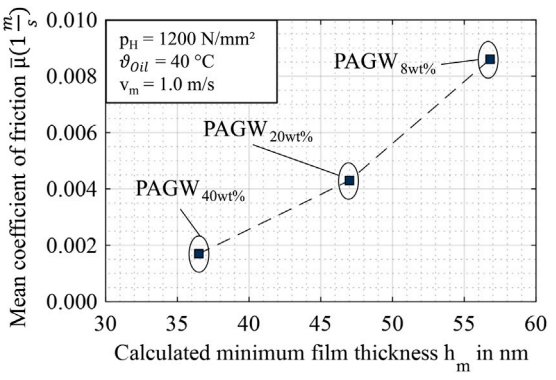

FIGURE 10
Mean coefficient of friction $\bar{\mu}$ (1 m/s) over calculated minimum film thickness h_m at p_H = 1200 N/mm² for the considered PAGWs.

TABLE 4 Calculated central, minimum and relative film thickness at v_m = 1.0 m/s and p_H = 1200 N/mm².

	$PAGW_{8wt\%}$	$PAGW_{20wt\%}$	$PAGW_{40wt\%}$	PAO-05
h_c in nm	94.7	77.3	59.3	104.3
h_m in nm	56.8	47.0	36.5	60.5
λ_{rel}	4.1	3.4	2.6	4.4

v_m = 1.0 m/s on the MTM2 tribometer is considered. Table 4 shows the calculated central (h_c) and minimum film thickness h_m as well as λ_{rel} for v_m = 1.0 m/s and p_H = 1200 N/mm². The lowest film thickness is calculated for $PAGW_{40wt\%}$ with λ_{rel} = 2.6, which is only slightly lower than the threshold for fluid film lubrication. Hence, the measured friction curves represent mainly the fluid friction in fluid film lubrication.

4.4 Trade-off between friction and film thickness

EHL friction and film thickness are strongly influenced by the water content of PAGWs. As a summary of the results, Figure 10 shows the mean coefficient of friction $\bar{\mu}$ (1 m/s) as a function of the calculated minimum film thickness h_m at a mean speed v_m = 1.0 m/s and contact pressure p_H = 1200 N/mm². The lowest coefficient of friction is associated with the lowest minimum film thickness. Thus, low water content in PAGWs results in higher lubricant film thickness but also higher friction and vice versa. However, superlubricity is achieved even for $PAGW_{8wt\%}$. Depending on the friction, film thickness and cooling requirements of a specific tribosystem, the water content of PAGWs can be chosen accordingly. If a given tribosystem operates at low speed and features a high surface roughness, the water content can be chosen low to support elastohydrodynamic lubricant film formation and to avoid wear. If a given tribosystem operates at higher speed and features a low surface roughness, the water content can be chosen high to use the full potential of friction reduction. Note, that the friction results correspond to the fluid film lubrication regime (see Section 4.3). The friction results for boundary and mixed lubrication might be considerably different.

5 Conclusion

Elastohydrodynamic fluid friction and film thickness were measured in rolling-sliding contacts using ball-on-disk tribometers to investigate the influence of the water content of water-containing PAGs. All lubricants including a reference PAO were of the same viscosity grade. The main conclusions can be summarized as follows.

1) The friction of water-containing PAGs is very low for all investigated water contents. Compared to the reference PAO, mean maximum friction reductions of 81%, 91% and 95% are found for water contents of 8 wt%, 20 wt% and 40 wt% respectively.
2) With increasing water content, the coefficient of friction decreases. For water contents of 20 wt% and 40 wt%, superlubricity is achieved for all considered operating conditions with maximum coefficients of friction at p_H = 1200 N/mm² of ≈ 0.007 and ≈ 0.004.
3) The characteristic of friction curves of water-containing PAGs differs from the reference PAO. An almost linear increase over the slide-to-roll ratio with negligible influence of contact pressure, speed and thermal effects is found.
4) All investigated water-containing PAGs are capable of lubricant film formation. The central film thickness decreases with increasing water content. Compared to the reference PAO, mean central film thickness reductions of 8%, 37% and 56% are found for water contents of 8 wt%, 20 wt% and 40 wt% respectively.
5) Although the pressure-viscosity coefficient of the reference PAO is approximate twice that of the water-containing PAG with 8 wt% water content, the central film thickness is similar. This can be attributed to the higher density of water-containing PAGs.
6) The water content of water-containing PAGs can be chosen dependent on the friction, film thickness and cooling requirements of a specific tribosystem.

In addition to the great potential of water-containing PAGs for elastohydrodynamic friction reduction with good lubricant film formation capability, their calorimetric properties are very promising, e.g., for a holistic thermal management in electrified vehicles. Nevertheless, water can evaporate and change the properties of the water-containing PAGs. Hence, the water content has to be kept within specified limits, which will be

investigated in a subsequent study. Further research may also focus on understanding the lubrication mechanisms of water-containing PAGs in more detail, e.g., by the use of molecular dynamic simulations.

Data availability statement

The original contributions presented in the study are included in the article/Supplementary Material, further inquiries can be directed to the corresponding author.

Author contributions

SH prepared the methodology, conducted the investigations and wrote the manuscript. TL reviewed and supervised the study and participated together with KS the scientific discussion. All authors proofread the manuscript.

Funding

The presented results are based on the research project CHEPHREN (03EN4005A) supported by the Federal Ministry for Economic Affairs and Climate Action (BMWK) and supervised by Project Management Jülich (PtJ).

Acknowledgments

The authors would like to thank for the sponsorship and support received from BMWK and PtJ.

Conflict of interest

The authors declare that the research was conducted in the absence of any commercial or financial relationships that could be construed as a potential conflict of interest.

Publisher's note

Supplementary material

The Supplementary Material for this article can be found online at: https://www.frontiersin.org/articles/10.3389/fmech.2023.1128447/full#supplementary-material

References

Bader, N., Wang, D., and Poll, G. (2017). Traction and local temperatures measured in an elastohydrodynamic lubrication contact. *Proceedings of the Institution of Mechanical Engineers, Part J: Journal of Engineering Tribology*. 231 (9), 1128–1139. doi:10.1177/1350650117713358

Burbank, J., Rausch, J., Luther, R., and Kraft, G. (2020). New approaches to extreme friction reductions with lubricants. *Proceedings of the* 22nd *International Colloquium Tribology*.

Chen, Z., Liu, Y., Zhang, S., and Luo, J. (2013). Controllable superlubricity of glycerol solution via environment humidity. *Langmuir* 29, 11924–11930. doi:10.1021/la402422h

Escobar, W. (2008). Understanding polyalkylene glycols (and where to apply them). *Tribology & Lubrication Technology*. 64 (5), 34–39.

Ge, X., Halmans, T., Li, J., and Luo, J. (2018). Molecular behaviors in thin film lubrication-Part three: Superlubricity attained by polar and nonpolar molecules. *Friction* 7, 625–636. doi:10.1007/s40544-018-0254-2

Ge, X., Li, J., and Luo, J. (2019). Macroscale superlubricity achieved with various liquid molecules: A review. *Frontiers in Mechanical Engineering*. 5 (2). doi:10.3389/fmech.2019.00002

Gohar, R. (2001). *Elastohydordynamics*. London, United Kingdom: John Wiley & Sons.

Habchi, W., Matta, C., Joly-Pottuz, L., Barros Bouchet, D.-I., Martin, J. M., and Vergne, P. (2011). Full film, boundary lubrication and tribochemistry in steel circular contacts lubricated with glycerol. *Tribology Letters*. 42, 351–358. doi:10.1007/s11249-011-9778-6

Hamrock, B. J., and Dowson, D. (1976). Isothermal elastohydrodynamic lubrication of point contacts: Part III—fully flooded results. *Journal of Lubrication Technology*. 99 (2), 264–275. doi:10.1115/1.3453074

Han, T., Zhang, S., and Zhang, C. (2022). Unlocking the secrets behind liquid superlubricity: A state-of-the-art review on phenomena and mechanisms. *Friction* 10 (8), 1137–1165. doi:10.1007/s40544-021-0586-1

Hartl, M., Krupka, I., and Liska, M. (1997). Differential colorimetry: Tool for evaluation of chromatic interference patterns. *Optical Engineering*. 36 (9), 2384. doi:10.1117/1.601415

Hirano, M., and Shinjo, K. (1990). Atomistic locking and friction. *Physical Review*. 41 (17), 11837–11851. doi:10.1103/PhysRevB.41.11837

Holmberg, K., and Erdemir, A. (2017). Influence of tribology on global energy consumption, costs and emissions. *Friction* 5, 263–284. doi:10.1007/s40544-017-0183-5

Li, J., Zhang, C., Ma, L., and Luo, J. (2013). Superlubricity achieved with mixtures of acids and glycerol. *Langmuir* 29, 271–275. doi:10.1021/la3046115

Liu, H. C., Zhang, B., Bader, N., Venner, C. H., and Poll, G. (2020). Scale and contact geometry effects on friction in thermal EHL: Twin-disc versus ball-on-disc. *Tribology International*. 154, 106694. doi:10.1016/j.triboint.2020.106694

Liu, W., Wang, H., Liu, Y., Li, J., Erdemir, A., and Luo, J. (2019). Mechanism of superlubricity conversion with polyalkylene glycol aqueous solutions. *Langmuir* 35, 11784–11790. doi:10.1021/acs.langmuir.9b01857

Luther, R. (2021). *Mehr Kühlen beim Schmieren: Wasserhaltige Getriebefluide für den elektrifizierten Antriebsstrang. Experten-Forum Powertrain: Reibung in Antrieb und Fahrzeug 2020. 203-208*. Berlin, Germany: Springer Vieweg.

Mayer, J. (2013). *Einfluss der Oberfläche und des Schmierstoffs auf das Reibungsverhalten im EHD-Kontakt*. Munich, Germany: Technical University of Munich. [dissertation]. [Munich].

Morhard, B., Schweigert, D., Mileti, M., Sedlmair, M., Lohner, T., and Stahl, K. (2021). Efficient lubrication of a high-speed electromechanical powertrain with holistic thermal management. *Forschung im Ingenieurwesen*. 85, 443–456. doi:10.1007/s10010-020-00423-0

Morhard, B., Schweigert, D., Paschold, C., Lohner, T., and Stahl, K. (2022). "Experimental results on the mechanical efficiency of the high-speed powertrain Speed4E," in CTI Symposium, Berlin. Germany, December 2022.

Omasta, M., Ebner, M., Sperka, P., Lohner, T., Krupka, I., Hartl, M., et al. (2018). Film formation in EHL contacts with oil-impregnated sintered materials. *Industrial Lubrication Technology*. 70 (4), 612–619. doi:10.1108/ILT-11-2017-0340

Sagraloff, N., Dobler, A., Tobie, T., Stahl, K., and Ostrowski, J. (2019). Development of an oil free water-based lubricant for gear applications. *Lubricants* 7 (4), 33. doi:10.3390/lubricants7040033

Schmidt, R., Klingelnberg, G., and Woydt, M. (2006). Thermophysical and viscosimetric properties of environmentally acceptable lubricants. *Industrial Lubrication and Tribology*. 58 (4), 210–224. doi:10.1108/00368790610670809

Schweigert, D., Gerlach, M. E., Hoffmann, A., Morhard, B., Tripps, A., Lohner, T., et al. (2020). On the impact of maximum speed on the power density of electromechanical powertrains. *Vehicles* 2 (2), 365–397. doi:10.3390/vehicles2020020

Sedlmair, M., Lohner, T., and Stahl, K. (2020). "Increasing gearbox efficiency of battery electric vehicles with water-containing gluids," in 61th German Tribology Conference, Göttingen, Germany, September 2020.

Shi, Y., Minami, I., Grahn, M., Björling, M., and Larsson, R. (2014). Boundary and elastohydrodynamic lubrication studies of glycerol aqueous solutions as green lubricants. *Tribology International*. 69, 39–45. doi:10.1016/j.triboint.2013.08.013

Spencer, N. D. (2014). Aqueous lubrication with poly(ethylene glycol) brushes. *Tribology Online*. 9, 143–153. doi:10.2474/trol.9.143

Tamayo, J. G. Z., Björling, M., Shi, Y., Parakash, B., and Larrson, R. (2022). Micropitting performance of glycerol-based lubricants under rolling-sliding contact conditions. *Tribology International*. 167, 107348. doi:10.1016/j.triboint.2021.107348

Voorst, R., and Alam, F. (2000). Polyglycols as base fluids for environmentally-friendly lubricants. *Journal of Synthetic Lubrication*. 16 (4), 313–322. doi:10.1002/jsl.3000160404

Wang, H., Liu, Y., Li, J., and Luo, J. (2016). Investigation of superlubricity achieved by polyalkylene glycol aqueous solutions. *Advanced Materials Interfaces*. 3 (19), 1600531. doi:10.1002/admi.201600531

Woydt, M. (2021). The importance of tribology for reducing CO_2 emissions and for sustainability. *Wear* 474-475, 203768. doi:10.1016/j.wear.2021.203768

Yilmaz, M., Mirza, M., Lohner, T., and Stahl, K. (2019a). Superlubricity in EHL contacts with water-containing gear fluids. *Lubricants* 7 (5), 46. doi:10.3390/lubricants7050046

Yilmaz, M., Lohner, T., Michaelis, K., and Stahl, K. (2019b). Minimizing gear friction with water-containing gear fluids. *Forschung im Ingenieurwesen*. 83 (3), 327–337. doi:10.1007/s10010-019-00373-2

Zhang, C. H., Zhao, Y. C., Björling, M., Wang, Y., Luo, J. B., and Prakash, B. (2012). EHL properties of polyalkylene glycols and their aqueous solutions. *Tribology Letters*. 45, 379–385. doi:10.1007/s11249-011-9883-6

Ziegltrum, A., Stahl, K., and Lohner, T. (2017). TEHL Simulation on the Influence of Lubricants on load-dependent gear losses. *Tribology International*. 111, 252–261. doi:10.1016/j.triboint.2016.12.018

Nomenclature

Parameter Unit Description

α_p 1/GPa Pressure-viscosity coefficient

E' N/mm² Reduced Young's modulus

h_c nm Central film thickness

$\bar{h}_c$ nm Mean central film thickness

h_m nm Minimum film thickness

G - Material parameter

p_H N/mm² Hertzian pressure

k - Ellipticity ratio

n - Refractive index

R mm Reduced radius of curvature

Ra µm Arithmetic surface roughness

Rq µm Root mean square surface roughness

SRR - Slide-to-roll ratio

v_m m/s Mean speed

v_g m/s Sliding speed

U - Speed parameter

W - Load parameter

ϑ_{Oil} °C Oil temperature

λ_{rel} - Relative film thickness

μ - Coefficient of friction

$\bar{\mu}$ - Mean coefficient of friction

μ_{max} - Maximum coefficient of friction